

Article

# Weak Deflection Angle, Hawking Radiation and Greybody Bound of Reissner–Nordström Black Hole Corrected by Bounce Parameter

Wajiha Javed <sup>1</sup>, Mehak Atique <sup>1</sup>, Reggie C. Pantig <sup>2</sup>  and Ali Övgün <sup>3,\*</sup> 

<sup>1</sup> Department of Mathematics, Division of Science and Technology, University of Education, Lahore 54590, Pakistan

<sup>2</sup> Physics Department, Mapúa University, 658 Muralla St., Intramuros, Manila 1002, Philippines

<sup>3</sup> Physics Department, Eastern Mediterranean University, North Cyprus via Mersin 10, Famagusta 99628, Turkey

\* Correspondence: ali.ovgun@emu.edu.tr

**Abstract:** In this study, we probe the weak lensing by a Reissner–Nordström black hole corrected by bounce parameter in plasma and dark matter mediums. For this, the optical geometry and the Gibbons–Werner approach are utilized to obtain the bending angle in the weak field limitations. We examine that the impact of these mediums increases the black hole’s bending angle. In addition, we graphically study the deflection angle of light with respect to the impact parameter and examine that the bounce parameter directly affects the angle. Further, we compute the Hawking radiation via a topological method involving two invariants and verify our obtained result with the standard method of calculating the Hawking temperature. In addition, we compute the greybody factor’s bound of the black hole. Moreover, we analyze the bound graphically and observe that the bound shows convergent behavior. We also study that our attained results reduce the results of the Reissner–Nordström and Schwarzschild black holes by reducing the parameters. Finally, we probe how the bounce parameter affected the shadow radius and compared it to the shadow produced if the black hole is immersed in plasma. It is revealed that the rate at which the shadow radius changes with respect to  $r$  easily tends to zero under the effect of the bounce parameter, while the plasma merely increases the shadow radius.

**Keywords:** general relativity; bending angle; Gauss–Bonnet theorem; plasma medium; black hole; greybody; Hawking temperature

**PACS:** 95.30.Sf; 98.62.Sb; 97.60.Lf



**Citation:** Javed, W.; Atique, M.; Pantig, R.C.; Övgün, A. Weak Deflection Angle, Hawking Radiation and Greybody Bound of Reissner–Nordström Black Hole Corrected by Bounce Parameter. *Symmetry* **2023**, *15*, 148. <https://doi.org/10.3390/sym15010148>

Academic Editors: André Maeder and Vesselin G. Gueorguiev

Received: 28 October 2022

Revised: 26 December 2022

Accepted: 1 January 2023

Published: 4 January 2023



**Copyright:** © 2023 by the authors. Licensee MDPI, Basel, Switzerland. This article is an open access article distributed under the terms and conditions of the Creative Commons Attribution (CC BY) license (<https://creativecommons.org/licenses/by/4.0/>).

## 1. Introduction

General relativity (GR) is the theory of gravity proposed by Einstein in 1916. In GR, Einstein gave the idea of black holes (BHs) [1]. Acknowledging Newton’s corpuscular theory of light, which assumed that photons are ultra-light particles, geologist Michell proposed the presence of dark stars. Today, these dark stars are known as BHs. Black holes are fascinating astronomical objects with a gravitational attraction so powerful that nothing can escape them, not even light. According to the no-hair theorem, all astrophysical BHs are fully defined by their masses and spins. A BH has two main components: the singularity and the event horizon. The question which attains the most attention in GR is about the inner structure of a BH. However, because of the presence of the spacetime singularity, where the curvature deviates continuously, and GR breaks down, this question cannot be answered easily. The singularity theorems, presented by Penrose and Hawking [2], state that gravitational collapse with physically valid circumstances always results in the formation of a singularity. Even in some scenarios (such as a cosmological constant in

the spacetime area), the singularity theorem's assumptions may not be applied. Black holes having regular centers or, in other words, having no singularity are called regular BHs or non-singular BHs. The first regular BH with horizons and no core singularity [3] was proposed by Bardeen [4]. Near the origin, the Bardeen BH behaves like a de Sitter spacetime, however, for  $r \rightarrow \infty$ , it acts like a Schwarzschild BH [3]. Later, Ayon-Beato and Garcia [5] showed that Bardeen's model is an accurate solution of GR connected to non-linear electrodynamics. There has been significant progress in the study and application of regular BHs [6–8], as well as regular rotating black holes [8,9]. Most of these solutions are based on Bardeen's concept, which uses non-linear electrodynamics as a source.

According to Hawking [10], a BH can emit heat radiation by taking into account the quantum consequences, and Hawking radiation is a term used to describe this type of heat radiation. The production and annihilation of particles are theoretically feasible in the context of quantum field theory. When pair creation occurs near the BH's horizon, one of the particles from the pair falls back to the BH while the other particles depart from the BH's horizon. The particles that exit are observed by an outside observer as Hawking radiation [11–13]. According to GR, the spacetime bend by a BH acts as a gravitational potential inside which the particles move. Some Hawking radiation is returned to the BH while the remainder passes through the potential at infinity. In this aspect, the transmission probability is known as the greybody factor. Several methods for obtaining Hawking radiation have been proposed. Using a topological method, Zhang, Wei, and Liu [14] investigated the Hawking temperature of the BTZ BH. Övgün et al. [15] computed the Hawking temperature for BHs by applying the topological strategy. Kruglov [16] explored the Hawking temperature of a magnetically charged BH through surface gravity and horizon in the context of non-linear electrodynamics. The greybody factor can be calculated in a variety of ways. The matching approach can be used to derive an estimated greybody factor [17–19]. The WKB approximation may be used to calculate the greybody factor if the gravitational potential is high enough [20,21]. The greybody factor may also be calculated using the rigorous bound, which is an alternative to approximation. The bound can be used to describe a BH qualitatively. Visser [22] inspected some extremely wide reflected and transmitted coefficient constraints for one-dimensional potential scattering. Boonserm and Visser [23] calculated the greybody factor's bound for Schwarzschild BHs by examining the Regge-Wheeler equation for wave phase angular momentum and arbitrary particle spin. Javed, Hussain, and Övgün [24] worked out the boundaries of the Kazakov Solodukhin BH's greybody factor.

The gravitational lensing (GL) effect states that a light beam would be distorted while passing by a huge object, which is one of GR's most important predictions. For determining the mass of galaxies and clusters [25,26], as well as discovering dark energy and dark matter (DM) [27], GL has become one of the most powerful instruments in astronomy and cosmology. Since the first measurements of the Sun's gravitational bending of light, the lens equation has been used to examine the GL effects for BHs, wormholes, cosmic strings, and other objects. Strong GL and weak GL are the types of GL. Strong GL is a GL effect that is intense enough to generate many pictures, such as arcs or Einstein's rings. In this type of GL, geometry is favorable and bending is rather large, whereas the weak GL is a GL impact that is not intense to create multiple pictures, and the geometry is less suitable. Since the 19th century, various studies on the GL have been done not only for the BHs but also for the wormholes, cosmic strings, global monopoles, and neutron stars [28–35].

Gibbons and Werner (GW) presented a technique for calculating the deflection angle in 2008. The Gauss-Bonnet theorem (GBT) and the optical geometry of the BH's spacetime, where the source and viewer are in asymptotic areas, were used to develop their technique. Werner [36] soon expanded this approach to stationary spacetimes. In GBT, one can utilize the domain  $\mathcal{G}_S$  confined by the light ray as well as a circular boundary curve  $\mathcal{C}_S$  placed at the lens's center where the light ray intersects at the source and receiver. The source and

receiver are considered at the same coordinate distance  $S$  from the lens. The GBT in optical metric and by using weak field approximation can be expressed as follows

$$\int \int_{\mathcal{G}_S} \tilde{\mathcal{K}} dS + \oint_{\partial \mathcal{G}_S} k dt + \sum_i \epsilon_i = 2\pi \mathcal{X}(\mathcal{G}_S), \quad (1)$$

wherein  $\tilde{\mathcal{K}}$  indicates the Gaussian optical curvature,  $k$  stands for geodesic curvature,  $dS$  is a surface element of optical geometry, and  $\mathcal{G}_S$  is a region accommodates the light rays source, the referential of the observer and the lens's center. At  $i$ th vertex,  $\epsilon_i$  represents the exterior angles. Just for simplicity, we suppose that as long as radial distance  $S \rightarrow \infty$ , the sum of the external angles  $\theta_i$  becomes  $\pi$  for the observer. The asymptotic deflection angle  $\tilde{\alpha}$  can be calculated as:

$$\tilde{\alpha} = - \int_0^\pi \int_{\frac{b}{\sin(\phi)}}^\infty \tilde{\mathcal{K}} dS, \quad (2)$$

where  $b$  represents the impact parameter. The integral of GBT may be solved in an infinite region confined by a ray of light. Instead of utilizing the asymptotic receiver and source, Ishihara et al. [37,38] modified this approach for finite distances. The finite-distances approach was then applied to the axisymmetric spacetimes by Ono et al. [39]. In the plasma medium, the GBT was used by Crisnejo, and Gallo [40] to determine the gravitational bending of light. Using massive particles and the Jacobi–Maupertuis Randers–Finsler metric inside GBT, Li et al. [41,42] investigated the finite-distance impacts on the weak bending angle.

Beginning from the first startling discoveries by Oort [43] of missing matter in the Galactic disk, which modern observations have not confirmed, and by Zwicky, [44] the discovery of missing matter in the Coma cluster, much later understood to be “DM”. Dark matter comprises particles that do not absorb, reflect, or emit light, making it impossible to detect them using electromagnetic radiation. Only gravitational interactions can detect DM, and we know that DM is non-baryonic, non-relativistic, and possesses weak non-gravitational interactions. Weakly interacting massive particles (WIMPs), super-WIMPs, axions, and sterile neutrinos are the four candidates of DM [45]. Dark matter constitutes about 85% of the total mass of the Universe [46] and is used to explain the strange behavior of stars and galaxy dynamics. In DM medium, Pantig and Övgün [47–51] studied the weak GL by wormholes and BHs.

The light that passes close to the BH is refracted by the gravitational field, creating the BH's shadow. The BH's shadow is a dark area frequently surrounded by a luminous ring. The BH's mass and angular momentum determine its size and form. Many scientists have attempted to predict how the observable appearance of a BH surrounded by bright material would seem before the spectacular finding of the BH's shadow produced by Event Horizon Telescope Collaboration [52,53]. For instance, Bardeen et al. [54] examined the shadows of Kerr BH's, while Synge [55] studied the shadows of Schwarzschild spacetime. The bright accretion disc surrounding the BH was manually drawn by Luminet [56]. In addition, due to the transparent emissions close to the BH, it is predicted that a BH would display its shadow, which is brought on by gravitational light deflection and photons captured at its event horizon. The photon ring, a geometric characteristic of spacetime, determines the shadow radius [57]. To our knowledge, few studies about RN black hole with bounce parameter have been conducted. For instance, [58] has considered the photon rings and shadows. In this study, we ought to analyze such a metric under the influence of plasma and dark matter. With the shadow cast, it can also determine imprints of spacetime, and several studies were also conducted about using the black hole for dark matter detection [50,51,59–68].

This paper aims to study the weak GL of black bounce Reissner–Nordström spacetime utilizing optical geometry and GBT in plasma and DM mediums. Moreover, it would be interesting to calculate the Hawking temperature and greybody bound of the BH. We will also study the graphical behavior of the deflection angle and greybody bound. We will

focus on how the bounce parameter (introduced in Reissner–Nordström BH) affects the bending angle, Hawking temperature, and the bound.

The layout of our paper is given as follows. Section 2 is based on the discussion about the black bounce Reissner–Nordström spacetime. In Section 3, we obtain the optical metric from a four-dimensional spherically symmetric metric and then compute the deflection angle of the BH with plasma medium by using GBT, and analyze its graphical behavior. The computation of the bending angle in the case of DM medium is given in Section 4. Section 5, is devoted to investigating the Hawking temperature of black bounce Reissner–Nordström BH via GBT. The computation of the greybody factor’s bound of black bounce Reissner–Nordström BH, and the graphical behavior of the bound is addressed in Section 6. Finally, Section 7 discusses the shadow behavior. The purpose of Section 8 is to sum up the findings of this research and propose a research direction. Throughout the paper, we used natural units  $G = c = 1$  and metric signature  $(-, +, +, +)$ .

## 2. Black Bounce Reissner–Nordström Spacetime

One of the most significant problems is the prediction of the spacetime singularity within a BH or at the start of the universe, which implies that the GR theory fails there. To address the singularity issue, Bardeen [4] was the first who put up the idea of regular BHs, which has continuously attracted scientific interest. It is convenient to consider the regular BH due to the problematic nature of spacetime’s singularities. Regular BHs are solutions of the gravity equations that have an event horizon but no singularities in spacetime. Based on the bounce and quantum corrections, a wide range of regular black hole solutions have been attained [69–71]. The black bounce spacetime smoothly interpolates among ordinary Schwarzschild BH and Morris–Thorne traversable wormhole [72]. It is noteworthy to remark that throughout the geometry is regular and one can have a distinct type of “regular BH”, where the “origin”  $r = 0$  can either be spacelike, null, or timelike, as long as the parameter  $a \neq 0$ . Additionally, it was demonstrated that the spacetime metric may be utilized to characterize several interesting physical circumstances, such as a developing black-bounce, a wormhole to black-bounce transfer, and the opposite black-bounce to wormhole transition. In Reissner–Nordström BH, a regularizing process was recently proposed [71], which does not produce a standard regular BH [73], such as the Bardeen or Hayward BHs, rather, it produces a charged regular BH called a black bounce Reissner–Nordström or charged black bounce. In a static spherically symmetric spacetime, the line-element for the black bounce Reissner–Nordström BH can be described as [74]

$$ds^2 = -f(r)dt^2 + \frac{dr^2}{f(r)} + h(r)^2(d\theta^2 + \sin^2\theta d\phi^2), \quad (3)$$

where the metric function  $f(r)$  and  $h(r)^2$  are defined as

$$f(r) = 1 - \frac{2m}{\sqrt{r^2 + a^2}} + \frac{Q^2}{r^2 + a^2} \quad \text{and} \quad h(r)^2 = r^2 + a^2.$$

In the metric function,  $m$  stands for the mass of the BH,  $Q$  indicates the charge, and  $a$  represents the bounce parameter of black bounce Reissner–Nordström. Several characteristics of the black bounce family have been thoroughly investigated [75,76]. Some properties are that the curvature singularities are absent from the black bounce family on a global scale and satisfy all observable weak field tests. Based on the values of charge  $Q$  and bounce parameter  $a$ , one can easily interpolate the Reissner–Nordström and Schwarzschild BHs. By taking charge  $Q \neq 0$  and bounce parameter  $a = 0$ , one can obtain the Reissner–Nordström BH. If we consider the charge  $Q = 0$  and bounce parameter  $a = 0$ , then we can obtain the Schwarzschild BH. The event horizon of the Reissner–Nordström BH corrected by bounce parameter can be computed by taking  $f(r) = 0$ .

$$r_h = \sqrt{(m + \sqrt{m^2 - Q^2})^2 - a^2}.$$

One can observe that a coordinate speed of light may be described in terms of radial null curves ( $ds^2 = d\theta = d\phi = 0$ ), since the radial coordinate  $r \in (-\infty, +\infty)$  [74]:

$$C(r) = \left| \frac{dr}{dt} \right| = f(r) = 1 - \frac{2m}{\sqrt{r^2 + a^2}} + \frac{Q^2}{r^2 + a^2}. \tag{4}$$

Thus in this spacetime, a sphere’s area at  $r$  (radial coordinate) has the following form  $A(r) = 4\pi h(r)^2$ . The wormhole throat is where the area is minimized, and by observing the state, one may determine where the throat is  $A'(r_0) = 0$ , where the throat’s location is represented by  $r_0$ . The wormhole throat’s radius is thus given by  $h_0 = h(r_0)$ . We now divide this geometry into three categories [74]:

1. The outer and inner horizon exist at  $r_h$  for  $a < (m + \sqrt{m^2 - Q^2})$  and  $|Q| < m$ . In this instance,  $\exists r_h \in R^*$  and  $c(r_h) = 0$ . Since light has a zero coordinate speed, it cannot escape the horizon. This geometry indicates a charged regular black hole with usual outer and inner horizons.
2. One can obtain one extremal horizon  $r_h = 0$ , when  $a = (m + \sqrt{m^2 - Q^2})$  and  $|Q| < m$ , and we know  $\exists r_h = 0$  and  $c(r_h) = 0$ . For this case, the geometry represents the extremal charged regular BH, which is the one-way charged traversable wormhole with single extremal null throat at  $r_h = 0$ .
3. For the case when,  $a > (m + \sqrt{m^2 - Q^2})$  and whether  $|Q| < m$  or  $|Q| > m$ , there is no horizons. So, we have  $\forall$  radial coordinate  $r \in (-\infty, +\infty)$  and  $c(r) \neq 0$ . This case represents a two-way charged traversable wormhole and the light can travel throughout the domain.

### 3. Plasma-Influenced Deflection Angle

Guo and Miao [74] have calculated the deflection angle by Reissner–Nordström BH corrected by bounce parameter in non-plasma medium utilizing GBT. Now, in this section, we see how the presence of a plasma affects the bending of light by black bounce Reissner–Nordström BH specified by charge  $Q$  and bounce parameter  $a$ . In the scenario of plasma medium, the refractive index for the black bounce Reissner–Nordström is described as [40].

$$n(r) = \sqrt{1 - \delta \left( 1 - \frac{2m}{\sqrt{r^2 + a^2}} + \frac{Q^2}{r^2 + a^2} \right)}, \tag{5}$$

where,  $\delta = \frac{\omega_e^2}{\omega_\infty^2}$  and the plasma parameters  $\omega_e$  and  $\omega_\infty$  represents electron plasma frequency and photon frequency as marked by the static investigator at infinity. For static spherically symmetric metric in Equation (3) assuming that the source of light and viewer are on the equatorial region ( $\theta = \frac{\pi}{2}$ ). Because we are working with null geodesics, we use ( $ds^2 = 0$ ) to find the appropriate optical metric.

$$opticalmetric = n^2 dt^2 = g_{pq} dx^p dx^q = n^2(r) \left[ \frac{1}{(f(r))^2} dr^2 + \frac{h(r)^2}{f(r)} d\phi^2 \right], \tag{6}$$

where,  $p, q \in \{1, 2\}$ . In order to determine the optical Gaussian curvature  $\tilde{\mathcal{K}}$  from the optical metric Equation (6), we use the following expression

$$\tilde{\mathcal{K}} = \frac{R}{2}, \tag{7}$$

where  $R$  is the Ricci scalar calculated using the optical metric. Utilizing Equation (7) the Gaussian optical curvature of the black bounce Reissner–Nordström BH in plasma medium is calculated as

$$\begin{aligned} \tilde{\mathcal{K}} \simeq & -\frac{2m}{r^3} + \frac{3Q^2}{r^4} - \frac{6mQ^2}{r^5} + \frac{5Q^2\omega_e^2}{r^4\omega_\infty^2} - \frac{3m\omega_e^2}{r^3\omega_\infty^2} \\ & - \frac{26mQ^2\omega_e^2}{r^5\omega_\infty^2} - \frac{12a^2Q^2}{r^6} - \frac{a^2}{r^4} + \frac{28a^2mQ^2}{r^7} + \frac{10a^2m}{r^5} - \frac{20a^2Q^2\omega_e^2}{r^6\omega_\infty^2} \\ & - \frac{a^2\omega_e^2}{r^4\omega_\infty^2} + \frac{115a^2mQ^2\omega_e^2}{r^7\omega_\infty^2} + \frac{31a^2m\omega_e^2}{2r^5\omega_\infty^2} + \mathcal{O}(m^2, a^4, Q^4). \end{aligned} \tag{8}$$

The obtained value of Gaussian optical curvature in Equation (8) will be used later to compute the bending angle. Now, to acquire the deflection angle of the black bounce Reissner–Nordström BH in a plasma medium, we make use of the GBT, which is defined as follows [77]

$$\int \int_{\mathcal{G}_S} \tilde{\mathcal{K}} dS + \oint_{\partial\mathcal{G}_S} k dt + \sum_i \epsilon_i = 2\pi\mathcal{X}(\mathcal{G}_S). \tag{9}$$

As in above equation,  $k$  describes the geodesic curvature which is defined as  $k = g(\nabla_{\dot{\gamma}}\dot{\gamma}, \ddot{\gamma})$  wherein  $g(\dot{\gamma}, \dot{\gamma}) = 1$ ,  $\ddot{\gamma}$  illustrates the unit acceleration vector. At  $i$ th vertex,  $\epsilon_i$  represents the external angle. As  $S \rightarrow \infty$ , the jump angles becomes  $\frac{\pi}{2}$  so that we obtain  $\theta_o + \theta_S \rightarrow \pi$ . Since  $\mathcal{G}_S$  is a non-singular region, the Euler characteristic  $\mathcal{X}(\mathcal{G}_S)$  is equal to 1, and the following result is obtained

$$\int \int_{\mathcal{G}_S} \tilde{\mathcal{K}} dS + \oint_{\partial\mathcal{G}_S} k dt + \epsilon_i = 2\pi\mathcal{X}(\mathcal{G}_S), \tag{10}$$

where  $\epsilon_i = \pi$  denotes the total angle of jumps, and since  $S \rightarrow 0$ , the effective element is acquired as

$$k(E_S) = |\nabla_{\dot{E}_S}\dot{E}_S|. \tag{11}$$

The geodesic curvature’s radial component is expressed as follows [77]:

$$(\nabla_{\dot{E}_S}\dot{E}_S)^r = \dot{E}_S^\phi \partial_\phi \dot{E}_S^r + \Gamma_{\phi\phi}^r (\dot{E}_S^\phi)^2. \tag{12}$$

For very large  $S$ , we obtain

$$(\nabla_{\dot{E}_S^r}\dot{E}_S^r) \rightarrow \frac{1}{S}. \tag{13}$$

It is asserted that the geodesic curvature is independent of topological defects, implying that  $k(E_S) \rightarrow \frac{1}{S}$ . Utilizing the optical metric given in Equation (6), one can write  $dt = Sd\phi$  and have  $k(E_S)dt = d\phi$ . Now, using all the above-obtained results and the straight line approximation  $r = \frac{b}{\sin\phi}$ . The bending angle  $\tilde{\alpha}$  can be calculated by using the formula below:

$$\tilde{\alpha} = - \int_0^\pi \int_{b/\sin\phi}^\infty \tilde{\mathcal{K}} dS, \tag{14}$$

where  $dS = \sqrt{detg} dr d\phi$ . Using Equation (14) and the value of optical Gaussian curvature Equation (8), the bending angle  $\tilde{\alpha}$  of the black bounce Reissner–Nordström in plasma medium up to the leading order terms is calculated as

$$\begin{aligned} \tilde{\alpha} \simeq & \frac{4m}{b} + \frac{2m\omega_e^2}{b\omega_\infty^2} - \frac{8mQ^2}{3b^3} - \frac{3\pi Q^2}{4b^2} + \frac{2mQ^2\omega_e^2}{b^3\omega_\infty^2} \\ & - \frac{\pi Q^2\omega_e^2}{2b^2\omega_\infty^2} - \frac{8a^2m}{3b^3} + \frac{a^2\pi}{4b^2} + \frac{64a^2mQ^2}{15b^5} + \frac{27a^2\pi Q^2}{32b^4} \\ & - \frac{4a^2m\omega_e^2}{3b^3\omega_\infty^2} - \frac{16a^2mQ^2\omega_e^2}{5b^5\omega_\infty^2} + \frac{9a^2\pi Q^2\omega_e^2}{16b^4\omega_\infty^2} + \mathcal{O}(m^2, a^4, Q^4). \end{aligned} \tag{15}$$

The above deflection angle depends on the mass  $m$ , charge  $Q$ , bounce parameter  $a$ , impact parameter  $b$  and the plasma parameters i.e.,  $\omega_e$  and  $\omega_\infty$ . The terms without the bounce parameter  $a$  and which contain charge are due to the charged nature of the BH.

The remaining terms are due to the corrections with the bounce parameter  $a$ . For  $a = 0$ , one can find the bending angle  $\tilde{\alpha}$  of a Reissner–Nordström BH in a plasma medium. By neglecting the charge and bounce parameter, the obtained angle  $\tilde{\alpha}$  reduces to the bending angle of the Schwarzschild BH. We also observe that the effect of the plasma increases the deflection angle. The bending angle is inversely proportional to the photon frequency, so the bending angle increase by lowering the photon frequency and assuming the electron frequency is fixed. Moreover, one can attain the bending angle in the case of non-plasma medium [74] if we take  $\omega_e = 0$  or  $(\delta \rightarrow 0)$  in the derived deflection angle in Equation (15). We also observe that the obtained deflection angle Equation (15) is directly proportional to the mass  $m$ , charge  $Q$ , bounce parameter  $a$ , and inversely proportional to the impact parameter  $b$ .

**Graphical Behaviour:** Now we look into the graphical behavior of the black bounce Reissner–Nordström BH’s deflection angle  $\tilde{\alpha}$  relative to the impact parameter  $b$ , for the fixed value of mass  $m$  and charge  $Q$ , while varying bounce parameter  $a$  and plasma term.

For fixed values of mass  $m$  and charge  $Q$ ,  $\frac{\omega_e}{\omega_\infty} = 0.1$  and varying the values of bounce parameter  $a$ , Figure 1 depicts the graph of deflection angle  $\tilde{\alpha}$  vs impact parameter  $b$ . For  $a \geq 0$ , we investigate that at the small values of impact parameter  $b$ , one can obtain the maximum value of the bending angle  $\tilde{\alpha}$ . As the value of  $b$  increases, the bending angle  $\tilde{\alpha}$  exponentially decreases and approaches zero. It is observed that for the small values of  $b$ , one can obtain the positive angle (deflection in the upward direction). Further, we examine that the bending angle  $\tilde{\alpha}$  shows the inverse relationship with the impact parameter  $b$ . Moreover, physically the bending angle  $\tilde{\alpha}$  represents the stable behavior.

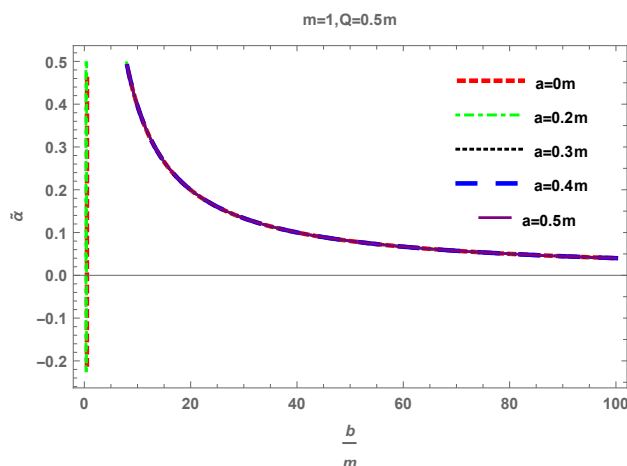


**Figure 1.** Bending angle’s variation  $\tilde{\alpha}$  as a function of impact parameter  $b$ .

Figure 2 depicts the behaviour of deflection angle  $\tilde{\alpha}$  with respect to the impact parameter  $b$  for  $Q = a = 0.5$  and  $0 \leq \frac{\omega_e}{\omega_\infty} \leq 1$ . We examine that the deflection angle  $\tilde{\alpha}$  decreases exponentially and almost approaches to zero as the value of impact parameter  $b$  goes to infinity. Furthermore, in this case, bending angle  $\tilde{\alpha}$  shows the inverse relation with the impact parameter  $b$ .

Figure 3 exhibits the behaviour of deflection angle  $\tilde{\alpha}$  with respect to impact parameter  $b$  for  $Q = a = 1$  and  $0 \leq \frac{\omega_e}{\omega_\infty} \leq 1$ . We examine that the deflection angle  $\tilde{\alpha}$  decreases exponentially and almost approaches to zero as the value of impact parameter  $b$  goes to infinity. In both cases ( $Q = a = 0.5, 1$ ), angle behavior is stable. It is observed that the for  $Q = 1$  deflection angle  $\tilde{\alpha}$  relative to the impact parameter  $b$  by varying bounce parameter  $a$  shows that similar behavior as for the  $Q = 0.5$ .

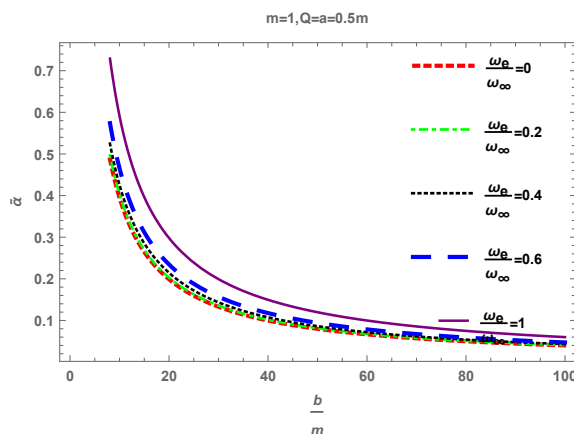


Figure 2. Bending angle’s variation  $\tilde{\alpha}$  as a function of impact parameter  $b$ , for  $Q = a = 0.5m$ .

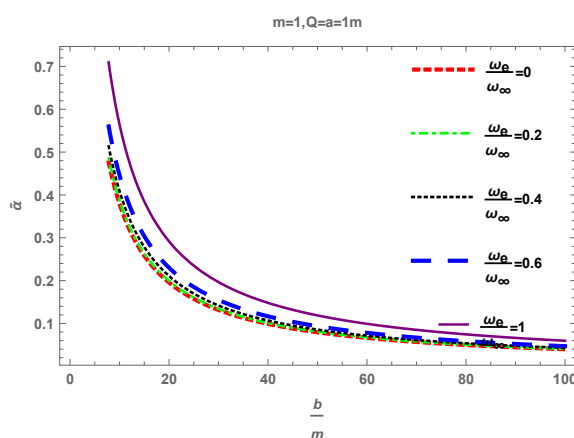


Figure 3. Bending angle’s variation  $\tilde{\alpha}$  as a function of impact parameter  $b$ ,  $Q = a = m$ .

#### 4. Dark Matter’s Influence on Deflection Angle

This section primarily concerns the calculations of black bounce Reissner–Nordström BH’s deflection angle in DM medium. The dark-atom concept has been offered as a composite of DM, which we study here using light’s bending phenomenon. Dark matter possesses electromagnetic interactions due to its frequency-dependent refractive index [78], and this medium has particular optical characteristics that a traveling photon may detect. The refractive index determines how fast a wave moves through a medium. In this regard, the refractive index for the black bounce Reissner–Nordström BH is defined as [78].

$$n(\omega) = 1 + \beta A_0 + A_2 \omega^2. \tag{16}$$

The frequency of a photon is represented by  $\omega$ . Here, it is examined that  $\beta = \frac{\rho_0}{4m^2\omega^2}$ , where  $\rho_0$  represents the mass density of dispersed particles of DM,  $A_0 = -2\varepsilon^2 e^2$  and  $A_2 \geq 0$ . The optical Gaussian curvature  $\tilde{\mathcal{K}}$  of the black bounce Reissner–Nordström BH in DM medium up to the leading order terms by using the Equation (7) can be calculated as

$$\begin{aligned} \tilde{\mathcal{K}} \simeq & \frac{3Q^2}{r^4(1 + A_2\omega^2 + A_0\beta)^2} - \frac{a^2}{r^4(1 + A_2\omega^2 + A_0\beta)^2} - \frac{12Q^2a^2}{r^6(1 + A_2\omega^2 + A_0\beta)^2} \\ & - \frac{2m}{r^3(1 + A_2\omega^2 + A_0\beta)^2} - \frac{6Q^2m}{r^5(1 + A_2\omega^2 + A_0\beta)^2} \\ & + \frac{10a^2m}{r^5(1 + A_2\omega^2 + A_0\beta)^2} + \frac{28Q^2a^2m}{r^7(1 + A_2\omega^2 + A_0\beta)^2} + \mathcal{O}(m^2, a^4, Q^4). \end{aligned} \tag{17}$$

The bending angle  $\tilde{\alpha}$  black bounce Reissner–Nordström BH in DM medium by using Equations (17) and (14) up to the leading order terms can be computed as

$$\begin{aligned}
\tilde{\alpha} \simeq & \frac{4m}{b(1+A_2\omega^2+A_0\beta)^2} - \frac{8a^2m}{3b^3(1+A_2\omega^2+A_0\beta)^2} + \frac{a^2\pi}{4b^2(1+A_2\omega^2+A_0\beta)^2} \\
& + \frac{64a^2mQ^2}{15b^5(1+A_2\omega^2+A_0\beta)^2} - \frac{8mQ^2}{3b^3(1+A_2\omega^2+A_0\beta)^2} + \frac{27a^2\pi Q^2}{32b^4(1+A_2\omega^2+A_0\beta)^2} \\
& - \frac{3\pi Q^2}{4b^2(1+A_2\omega^2+A_0\beta)^2} - \frac{16a^2mA_2\omega^2}{3b^3(1+A_2\omega^2+A_0\beta)^2} + \frac{8mA_2\omega^2}{b(1+A_2\omega^2+A_0\beta)^2} \\
& + \frac{a^2\pi A_2\omega^2}{2b^2(1+A_2\omega^2+A_0\beta)^2} + \frac{128a^2mQ^2A_2\omega^2}{15b^5(1+A_2\omega^2+A_0\beta)^2} - \frac{16mQ^2A_2\omega^2}{3b^3(1+A_2\omega^2+A_0\beta)^2} \\
& + \frac{27a^2\pi Q^2A_2\omega^2}{16b^4(1+A_2\omega^2+A_0\beta)^2} - \frac{3\pi Q^2A_2\omega^2}{2b^2(1+A_2\omega^2+A_0\beta)^2} \\
& + \mathcal{O}(m^2, a^4, Q^4, A_2^2, \omega^4).
\end{aligned} \tag{18}$$

The BH's mass  $m$ , charge  $Q$ , bounce parameter  $a$ , impact parameter  $b$ , and DM parameters all are the parameters of the measured deflection angle in Equation (18). It is to be observed that the photon deflected through the DM around the black bounce Reissner–Nordström BH has a large bending angle as compared to the vacuum case [74]. By eliminating the DM effect, the angle Equation (18) reduces to the bending angle in the case of vacuum. By considering  $Q \neq 0$  and  $a = 0$  in Equation (18), one can obtain the expression of the Reissner–Nordström BH's deflection angle. We also find that taking charge  $Q = 0$  and  $a = 0$  in Equation (18) the obtained angle reduces to the Schwarzschild BH's deflection angle in DM medium.

## 5. Hawking Radiation

Plot is needed here according to the 3rd referee. In this part, we use a topological technique based on the GBT and Euler characteristic to derive the Hawking temperature of a black bounce Reissner–Nordström BH. To derive the Hawking temperature using the topological approach, one can utilize the Wick rotation [79] to use the Euclidean geometry of the two-dimensional spacetime without missing any facts from the four-dimensional spacetime. The spherically static symmetric spacetime of black bounce Reissner–Nordström BH is defined in Equation (3).

Rewriting the four-dimensional metric into the two-dimensional coordinates by using the Wick rotation condition i.e.,  $(\theta = \frac{\pi}{2})$  and  $(\tau = it)$

$$ds^2 = \left(1 - \frac{2m}{\sqrt{r^2+a^2}} + \frac{Q^2}{r^2+a^2}\right) d\tau^2 + \frac{1}{\left(1 - \frac{2m}{\sqrt{r^2+a^2}} + \frac{Q^2}{r^2+a^2}\right)} dr^2. \tag{19}$$

The formula to compute the Hawking temperature  $T_H$  of black bounce Reissner–Nordström BH after using all the values of the physical constants is defined as [15]

$$T_H = \frac{1}{4\pi\mathcal{X}} \int_{r_h} \sqrt{g}\mathcal{R}dr, \tag{20}$$

where,  $g = 1$  is the determinant of Equation (19) and  $r_h$  is the event horizon. Using the values of Ricci scalar  $R$ , Euler characteristic  $\mathcal{X} = 1$  and integrating along the event horizon, the Hawking temperature  $T_H$  of black bounce Reissner–Nordström BH is calculated as

$$T_H = \frac{\sqrt{(m+\sqrt{m^2-Q^2})^2 - a^2}\sqrt{m^2-Q^2}}{2\pi(m+\sqrt{m^2-Q^2})^3}. \tag{21}$$

One can observe that the obtained expression of the Hawking temperature  $T_H$  black bounce Reissner–Nordström BH depends on the mass  $m$ , charge  $Q$  of the BH, and bounce

parameter  $a$  similarly with [71]. We also notice that the Hawking temperature via standard technique gives the same expression as the topological technique. For the case  $Q \neq 0$  and  $a = 0$ , the obtained Hawking temperature in Equation (21) reduces to the Hawking temperature of Reissner–Nordström BH. Moreover, the attained Hawking temperature Equation (21) reduces to the Schwarzschild–Hawking temperature, i.e.,  $T_H = \frac{1}{8m\pi}$  by taking  $Q = a = 0$ . To observe the behavior of Hawking temperature graphically, we plot the graph between Hawking temperature  $T_H$  and bounce parameter  $a$  in Figure 4. We observe that for  $Q = 0.5$  the Hawking temperature decreases exponentially.

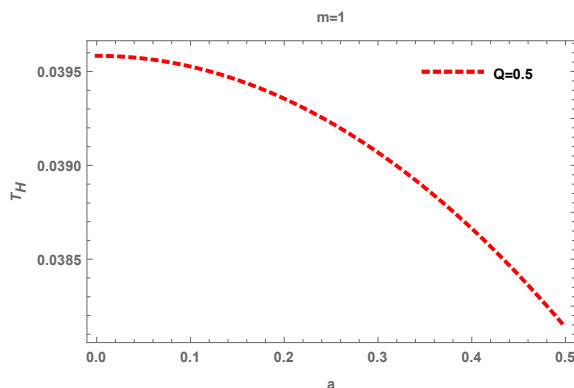


Figure 4. Hawking Temperature  $T_H$  vs the bounce parameter  $a$ .

### 6. Greybody Factor

This section mainly examines the greybody factor bound of the black bounce Reissner–Nordström BH. Much research has been dedicated to estimating the greybody factors. There is, however, a distinct analytic approach for obtaining bounds on the greybody components. The line-element for the Reissner–Nordström BH corrected by bounce parameter in a static spherically symmetric spacetime is defined in Equation (3) The lower bounds on transmission probability  $T$  can be defined as [22,80,81].

$$T \geq \operatorname{sech}^2 \left( \frac{1}{2\omega} \int_{-\infty}^{\infty} \varrho dr_* \right), \tag{22}$$

where

$$\varrho = \frac{\sqrt{[g'(r_*)]^2 + [\omega^2 - \mathcal{V}(r_*) - g^2(r_*)]^2}}{2g(r_*)}.$$

where  $r_*$  represents the tortoise coordinate, and  $g$  is a positive function. For the radial part, the equation of motion is given as

$$\frac{1}{h(r)^2} \frac{d}{dr} \left[ h(r)^2 f(r) \frac{du(r)}{dr} \right] + \left[ \frac{\omega^2}{f(r)} - \frac{l(l+1)}{h(r)^2} \right] u(r) = 0, \tag{23}$$

where  $u(r)$  indicates the the scalar or vector field oscillating. Taking  $dr_* = \frac{1}{f(r)} dr$ , while the potential is defined as [82]

$$\mathcal{V}(r) = \frac{l(l+1)f(r)}{h(r)^2}. \tag{24}$$

The lower bounds on the transmission probability  $T$  for  $g = \omega$  are given by

$$T \geq \operatorname{sech}^2 \left( \frac{1}{2\omega} \int_{r_h}^{\infty} \mathcal{V}(r) dr_* \right). \tag{25}$$

After substituting in the values of  $\mathcal{V}$  and  $dr_*$ , we obtain the following expression

$$T \geq \text{sech}^2 \left( \frac{1}{2\omega} \int_{r_h}^{\infty} \frac{l(l+1)}{h(r)^2} dr \right). \tag{26}$$

The greybody bound  $T_b$  of the black bounce Reissner–Nordström BH after putting the value of  $h(r)^2$  and integrating along  $r_h$  is calculated as

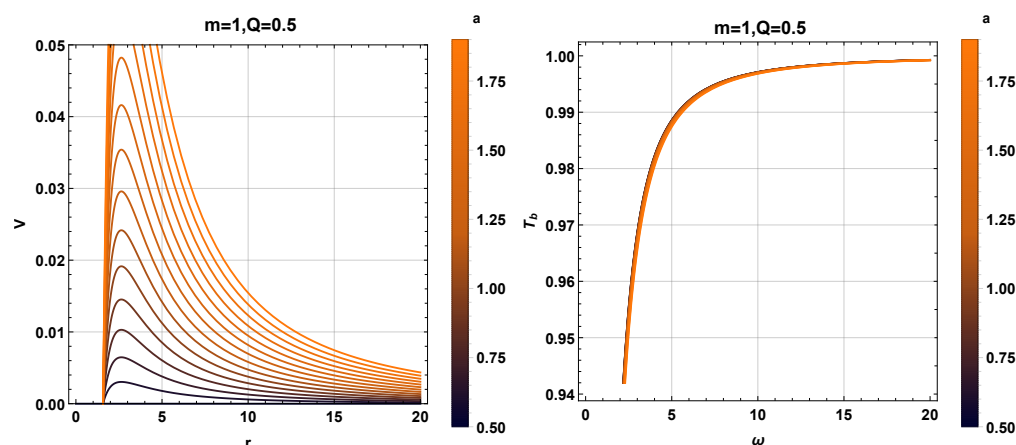
$$T_b = T \geq \text{sech}^2 \left[ \frac{1}{2\omega} \left( \frac{l(l+1)\pi}{2a} - \frac{l(l+1) \arctan \left[ \frac{\sqrt{(m+\sqrt{m^2-Q^2})^2-a^2}}{a} \right]}{a} \right) \right] \tag{27}$$

The bound  $T_b$  of the black bounce Reissner–Nordström BH depends upon the mass  $m$ , charge  $Q$ , and bounce parameter  $a$  of the BH. Guo and Miao [74] have also calculated the greybody factor of perturbation fields of the black bounce Reissner–Nordström BH. It is observed from the graphs that when the potential of the black bounce Reissner–Nordström BH is higher, then the bound will be lower.

*Graphical Analysis*

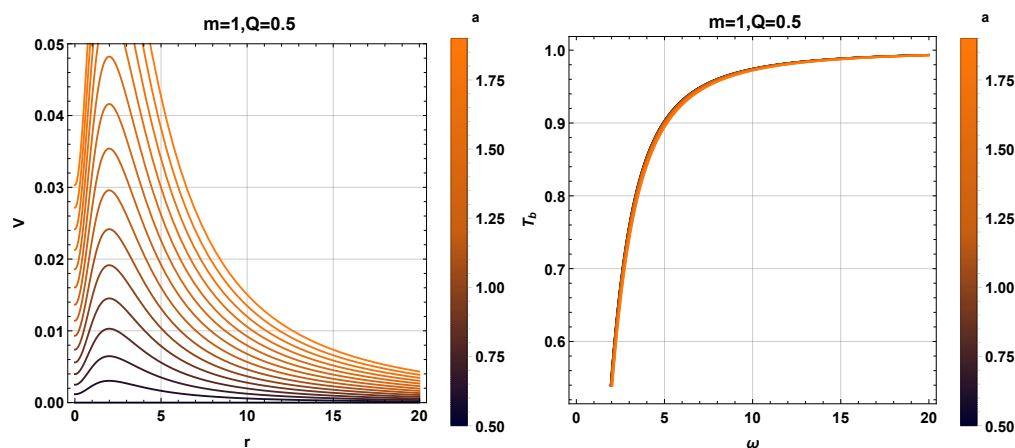
The purpose of this section is to explain the graphical behavior of greybody bound  $T_b$  and the potential of the black bounce Reissner–Nordström BH. For this purpose, we take the fixed values of charge  $Q$ , angular momentum  $l = 1, 2$ , and varying bounce parameter  $a$ .

Figure 5 depicts the graphical behavior of the potential  $\mathcal{V}$  relative to the  $r$ , and greybody factor bound  $T_b$  relative to the  $\omega$ . For  $0 < a < 2$ , the potential  $\mathcal{V}$  increases, and attains its maximum value. However, as the value of bounce parameter  $a \rightarrow 0$ , the potential exponentially decreases and approaches zero. It is also observed that as the  $r \rightarrow 0$ , the value of potential is high and attains its maximum value, while for the large values of  $r$  the potential starts decreasing from the maximum value and almost approaches zero. Nevertheless, as the value of  $a$  increases, the corresponding bound becomes lower, making it more difficult for the waves to pass through the higher potential. However, the bound  $T_b$  shows the convergent behavior by converging to 1.



**Figure 5.** The left panel shows the potential with  $l = 1$  and corresponding bound  $T_b$  is shown in right panel.

Figure 6 represents the graphical behavior of the potential  $\mathcal{V}$  with respect to the  $r$  and greybody factor bound  $T$  with respect to the  $\omega$ . For  $0 < a < 2$ , the bound  $T$  shows a similar behavior as for the  $l = 1$ .



**Figure 6.** The left panel shows the potential with  $l = 2$  and corresponding bound  $T_b$  is shown in right panel.

### 7. Shadow Behavior

We now turn our attention to the explore the shadow behavior of the black bounce RN black hole. Let us consider the Hamiltonian for light rays where a non-magnetized cold plasma with plasma frequency  $\omega_p(r)$  is included [83]:

$$H = \frac{1}{2} \left( g^{ik} p_i p_k + \omega_p(r)^2 \right) = \frac{1}{2} \left( -\frac{p_t^2}{A(r)} + \frac{p_r^2}{B(r)} + \frac{p_\phi^2}{C(r)} + \omega_p(r)^2 \right). \tag{28}$$

In the equation above, note that  $C(r) = h(r)^2$  due to Equation (3). Furthermore, we should also note that  $A(r) = f(r)$ , and  $B(r) = A(r)^{-1}$ . Without compromising generality, we can also restrict ourselves along the equatorial plane ( $\theta = \pi/2$ ) due to spherical symmetry and derive the equations of motions (EoS) through the following

$$\dot{x}^i = \frac{\partial H}{\partial p_i}, \quad \dot{p}_i = -\frac{\partial H}{\partial x^i}, \tag{29}$$

which reveals two constants of motion:

$$E = A(r) \frac{dt}{d\lambda}, \quad L = h(r)^2 \frac{d\phi}{d\lambda}. \tag{30}$$

With the above equation, we can define the impact parameter as

$$b \equiv \frac{L}{E} = \frac{h(r)^2}{A(r)} \frac{d\phi}{dt}, \tag{31}$$

and the condition that  $ds^2 = 0$ , gives the rate of change of the  $r$ -coordinate with respect to the azimuthal angle  $\phi$ :

$$\left( \frac{dr}{d\phi} \right)^2 = \frac{h(r)^2}{B(r)} \left( \frac{p(r)^2}{b^2} - 1 \right), \tag{32}$$

where [83]

$$p(r)^2 = \frac{h(r)^2}{A(r)} n(r)^2 = \frac{h(r)^2}{A(r)} \left( 1 - \frac{\omega_e^2}{\omega_0^2} A(r) \right) \tag{33}$$

since the non-gravitating plasma is assumed to be non-homogenous. With our metric functions, the condition  $p'(r) = 0$  allows one to find the photonsphere radius [83], and for our case,

$$\left( \frac{\omega_e^2}{\omega_0^2} A(r)^2 - A(r) \right) h'(r)^2 + h(r)^2 A'(r) = 0. \tag{34}$$

With the inclusion of the plasma parameter, finding the analytical expression for  $r_{ph}$  can be quite lengthy. However, for the case where there is no plasma (i.e.,  $n(r) = 1$ ), we simply found the physical solutions as

$$r_{ph} = \frac{\sqrt{18M^2 - 8Q^2 - 4a^2 + 6\sqrt{9M^4 - 8M^2Q^2}}}{2}. \tag{35}$$

A static observer at a distance  $r_{obs}$  from the black bounce black hole can obtain the angular radius  $\alpha_{sh}$  of the shadow. From the black hole’s center to  $r_{obs}$ , simple geometry shows that  $\Delta x = \sqrt{B(r)}dr$  and  $\Delta y = h(r)d\phi$  [83]:

$$\tan(\alpha_{sh}) = \lim_{\Delta x \rightarrow 0} \frac{\Delta y}{\Delta x} = h(r) \left( \frac{1}{B(r)} \right)^{1/2} \frac{d\phi}{dr} \Big|_{r=r_{obs}}, \tag{36}$$

which can be simplified in terms of the critical impact parameter as

$$\sin^2(\alpha_{sh}) = \frac{b_{crit}^2}{p(r_{obs})^2}. \tag{37}$$

Here, the  $b_{crit}$  can be obtained using the orbit equation [84]:

$$b_{crit}^2 = \frac{p(r_{ph}) \left( 2h(r_{ph})^2 B(r_{ph}) p'(r_{ph}) - h(r_{ph})^2 B'(r_{ph}) p(r_{ph}) + B(r_{ph}) h'(r_{ph})^2 p(r_{ph}) \right)}{B(r_{ph}) h'(r_{ph})^2 - h(r_{ph})^2 B'(r_{ph})} \tag{38}$$

The critical impact parameter’s analytical expression with  $n(r)$  is somewhat complicated, but for the case  $n(r) = 1$ , we find

$$b_{crit}^2 = \frac{2h(r_{ph})^3}{h(r_{ph}) - m}. \tag{39}$$

Finally, it can be easily shown that, in terms of  $r_{obs}$  and  $r_{ph}$ , we obtain the shadow radius as ( $n(r) = 1$ )

$$R_{sh} = \left[ \frac{2h(r_{ph})^3 (h(r_{obs})^2 - 2mh(r_{obs}) + Q^2)}{h(r_{obs})^2 (h(r_{ph}) - m)} \right]^{1/2}. \tag{40}$$

Next, we plotted Equation (40), which is indicated by the dotted lines in Figure 7. We also included in the plot the case where the black hole bounce is surrounded by plasma (solid lines). For immediate comparison, we also plotted the Schwarzschild and RN cases.

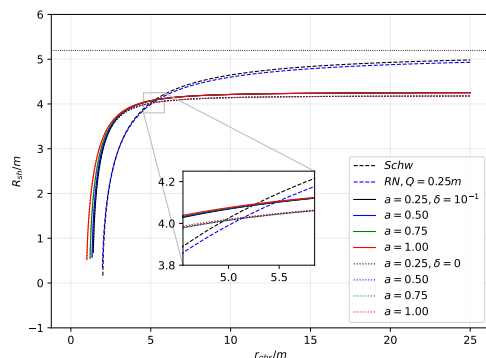


**Figure 7.** behavior of the shadow radius due to a static observer with varying location from the black bounce RN BH. Here, we used  $Q = 0.25m$ .

Furthermore, while it is understood that the shadow cast by a non-spinning black hole is a circle, we can see in the plot the behavior of the shadow radius. First, without the bounce parameter, the RN case with  $Q = 0.25m$  decreases the shadow radius while following the general trend of the Schwarzschild case. For the Schwarzschild case,  $R_{sh} = 3\sqrt{3}m$  as  $r_{obs}$  becomes larger, but at  $r_{obs} = 25m$ , we observe that it is still lower than this value of  $R_{sh}$ . The effect of the bounce parameter is to produce lower values of  $R_{sh}$  and make its rate of change with respect to  $r \rightarrow 0$  at lower values of  $r_{obs}$ . It means that the observer does not need to go so far away to observe a constant shadow radius. Furthermore, the bounce parameter allows the formation of the shadow near the event horizon. With the plasma medium  $\delta = 10^{-1}$ , we observe that  $r_{obs}$  follows the general trend for  $\delta = 0$ , but increases the shadow slightly. Such an increase depends on the value of the plasma parameter.

For completion, let us analyze the effect of the dark matter refractive index  $n(\omega)$  in Equation (16) instead of the plasma. The photonsphere can be found via

$$n(\omega)^2[h'(r)A(r) - A'(r)h(r)] = 0, \tag{41}$$

which reveals that the photonsphere radius is independent of the dark matter parameter. It is easy to see that through the orbit equation, one can verify that the critical impact parameter in this case is

$$b_{crit}^2 = \frac{2n(\omega)^2h(r_{ph})^3}{h(r_{ph}) - m}. \tag{42}$$

Then, the shadow is given by

$$R_{sh} = n(\omega)h(r_{ph}) \left[ \frac{2h(r_{ph})(h(r_{obs})^2 - 2mh(r_{obs}) + Q^2)}{h(r_{obs})^2(h(r_{ph}) - m)} \right]^{1/2}, \tag{43}$$

where the shadow radius is increased by a factor of  $n(\omega)$ .

### 8. Conclusions

In this work, we have discussed the Reissner–Nordström BH corrected by bounce parameter and its properties, i.e., the curvature singularities are absent from the black bounce family on a global scale and satisfy all observable weak field tests. In the case of plasma and DM mediums, the attained bending angle Equation (15) depended on the mass  $m$ , charge  $Q$  of the BH, bounce parameter  $a$ , impact parameter, and medium’s parameters. It is noted that in bending angle Equation (15) the terms without the bounce parameter  $a$  and which contain charge are due to the charged nature of the BH and the remaining terms are due to the corrections with the bounce parameter  $a$ . It is also found that the effect of the plasma increases the deflection angle. The bending angle is inversely proportional to the photon frequency, so the bending angle increases by lowering the photon frequency and assuming the electron frequency is fixed. It is to be observed that black bounce Reissner–Nordström BH’s bending angle increases due to the DM medium effect compared to the vacuum case.

In above both mediums, we have examined that in the absence of a bounce parameter, one can obtain the bending angle of Reissner–Nordström BH and the bending angle of Schwarzschild’s BH by neglecting the charge and bounce parameter of the BH. Moreover, one can attain the bending angle of a non-plasma medium by taking  $\omega_e = 0$  in a plasma medium. It is noticed that also that, by ignoring the DM effect in the angle of deflection in Equation (15), the angle reduces to the angle of a non-plasma medium. We also observed that the obtained bending angle in both mediums is directly proportional to the mass  $m$ , charge  $Q$ , bounce parameter  $a$ , and inversely proportional to the impact parameter  $b$ .

Following that, we have analyzed the graphical behavior of the bending angle  $\tilde{\alpha}$  with respect to the  $b$  for fixed values of mass  $m$ , charge  $Q$ ,  $\frac{\omega_e}{\omega_\infty} = 0.1$  and varying the value of bounce parameter  $a$ . We have examined that for at the small values of impact parameter  $b$ , the value of the bending angle  $\tilde{\alpha}$  is maximum and as the value of  $b$  increases, the bending

angle  $\tilde{\alpha}$  exponentially decreases and approaches to zero. Moreover, we have investigated the deflection angle  $\tilde{\alpha}$  with respect to the impact parameter  $b$  by fixing  $m, Q$ , taking  $a = 0.5, 1$  and varying the plasma factor. For  $Q = a = 0.5, 1$ , we have studied that the deflection angle  $\tilde{\alpha}$  decreases exponentially and almost approaches zero as the value of impact parameter  $b$  goes to infinity. In all the above cases, graphically we have observed that the deflection angle  $\tilde{\alpha}$  shows the inverse relationship with the impact parameter  $b$  and also the behavior of angle is physically stable.

Furthermore, we have computed the Hawking temperature using a topological method involving two invariants, namely the two-dimensional Euler characteristic and the GBT. We have examined that the obtained expression of the Hawking temperature  $T_H$  in Equation (21) black bounce Reissner–Nordström BH depends on the mass  $m$ , charge  $Q$  of the BH and bounce parameter  $a$ . We also noticed that the Hawking temperature expression is similar to the topological technique. It is to be mentioned here that for the case  $Q \neq 0$  and  $a = 0$ , the Hawking temperature Equation (21) reduces to the Hawking temperature of Reissner–Nordström BH, and for  $Q = a = 0$ , the acquired Hawking temperature converts to the Schwarzschild Hawking temperature, i.e.,  $T_H = \frac{1}{8m\pi}$ . Furthermore, we graphically investigated that the Hawking temperature decreases exponentially.

We have also calculated the greybody bound  $T_b$  and examined that the bound  $T_b$  of the black bounce Reissner–Nordström BH depends on the mass  $m$ , charge  $Q$  of the BH, and bounce parameter  $a$ . Moreover, we have observed that the potential  $\mathcal{V}$  increases and attains its maximum value for  $l = 1, 2$ . As the value of  $a$  increases, the potential exponentially decreases and approaches zero. It is to be mentioned here that when  $r \rightarrow 0$ , one can attain the high value of potential, and for the large value of  $r$  the potential approaches zero. It is observed that the corresponding bound becomes lower as the value of  $a$  increases. Furthermore, it is examined that the greybody factor's bound exhibits the convergent behavior and converges to 1. We also observed that for large values of  $a$  and small  $r$ , the potential is higher, making it difficult for the waves to pass through that potential.

Finally, we also explored the effect of the bounce parameter on the behavior of the shadow radius and when it is surrounded by plasma. First, the effect of the bounce parameter is to allow shadow formation closer to the black hole shadow and at a larger radius than the Schwarzschild or RN cases. Here, the rate at which the shadow increases is also larger. Moreover, we observe that the bounce parameter quickly makes the shadow radius rate of change tend to zero even at low values of  $r_{\text{obs}}$ . Finally, the effect of the plasma is just to increase the shadow radius of the black hole affected by the bounce parameter. These parameters can indeed change the shadow radius, which sophisticated astronomical devices can detect.

**Author Contributions:** Conceptualization, W.J. and A.Ö.; methodology, R.C.P. and A.Ö.; software, M.A.; validation, W.J., R.C.P. and A.Ö.; formal analysis, M.A.; investigation, M.A.; resources, W.J. and A.Ö.; writing—original draft preparation, M.A.; writing—review and editing, W.J., M.A., R.C.P. and A.Ö.; visualization, M.A. and R.C.P.; supervision, W.J. and A.Ö. All authors have read and agreed to the published version of the manuscript.

**Funding:** This research received no external funding.

**Institutional Review Board Statement:** Not applicable.

**Informed Consent Statement:** Not applicable.

**Data Availability Statement:** Not applicable.

**Acknowledgments:** A.Ö. and R.C.P. would like to acknowledge networking support by the COST Action CA18108—Quantum gravity phenomenology in the multi-messenger approach (QG-MM).

**Conflicts of Interest:** The authors declare no conflict of interest.

## References

1. Einstein, A. Lens-Like Action of a Star by the Deviation of Light in the Gravitational Field. *Science* **1936**, *84*, 506–507. <https://doi.org/10.1126/science.84.2188.506>.
2. Penrose, R. Gravitational Collapse and Space-Time Singularities. *Phys. Rev. Lett.* **1965**, *14*, 57–59. <https://doi.org/10.1103/PhysRevLett.14.57>.
3. Ansoldi, S. Spherical black holes with regular center: A Review of existing models including a recent realization with Gaussian sources. In Proceedings of the Conference on Black Holes and Naked Singularities, Milan, Italy, 10–12 May 2007.
4. Bardeen, J.M. Non-singular general-relativistic gravitational collapse. In Proceedings of the International Conference GR5, Tbilisi, GA, USA, 9–13 September 1968; p. 174.
5. Ayon-Beato, E.; Garcia, A. New regular black hole solution from nonlinear electrodynamics. *Phys. Lett. B* **1999**, *464*, 25–29.
6. Dymnikova, I. Vacuum nonsingular black hole. *Gen. Relat. Gravit.* **1992**, *24*, 235–242.
7. Lemos, J.P.S.; Zanchin, V.T. Regular black holes: Electrically charged solutions, Reissner-Nordström outside a de Sitter core. *Phys. Rev. D* **2011**, *83*, 124005. <https://doi.org/10.1103/PhysRevD.83.124005>.
8. Kumar, A.; Ghosh, S.G.; Maharaj, S.D. Nonsingular black hole chemistry. *Phys. Dark Universe* **2020**, *30*, 100634. <https://doi.org/10.1016/j.dark.2020.100634>.
9. Eichhorn, A.; Held, A. Image features of spinning regular black holes based on a locality principle. *Eur. Phys. J. C* **2021**, *81*, 933.
10. Hawking, S.W. Particle creation by black holes. *Commun. Math. Phys.* **1975**, *43*. <https://doi.org/10.1007/BF02345020>.
11. Hassanabadi, H.; Chung, W.S.; Lütfüoğlu, B.C.; Maghsoodi, E. Effects of a new extended uncertainty principle on Schwarzschild and Reissner-Nordström black holes thermodynamics. *Int. J. Mod. Phys. A* **2021**, *36*, 2150036. <https://doi.org/10.1142/S0217751X21500366>.
12. Hassanabadi, S.; Kříž, J.; Chung, W.S.; Lütfüoğlu, B.C.; Maghsoodi, E.; Hassanabadi, H. Thermodynamics of the Schwarzschild and Reissner-Nordström black holes under higher-order generalized uncertainty principle. *Eur. Phys. J. Plus* **2021**, *136*, 918. <https://doi.org/10.1140/epjp/s13360-021-01933-8>.
13. Chen, H.; Lütfüoğlu, B.C.; Hassanabadi, H.; Long, Z.W. Thermodynamics of the Reissner-Nordström black hole with quintessence matter on the EGP framework. *Phys. Lett. B* **2022**, *827*, 136994. <https://doi.org/10.1016/j.physletb.2022.136994>.
14. Zhang, Yu-Peng, S.W.W.; Liu, Y.X. Topological approach to derive the global Hawking temperature of (massive) BTZ black hole. *Phys. Lett. B* **2020**, *810*, 135788.
15. Övgün, A.; Sakalli, I. Hawking radiation via Gauss-Bonnet theorem. *Ann. Phys.* **2020**, *413*, 168071. <https://doi.org/10.1016/j.aop.2020.168071>.
16. Kruglov, S.I. Magnetically charged black hole in framework of nonlinear electrodynamics model. *Int. J. Mod. Phys. A* **2018**, *33*, 1850023.
17. Fernando, S. Greybody factors of charged dilaton black holes in 2 + 1 dimensions. *Gen. Relativ. Gravit.* **2005**, *37*, 461–481. <https://doi.org/10.1007/s10714-005-0035-x>.
18. Kim, W.; Oh, J.J. Greybody Factor and Hawking Radiation of Charged Dilatonic Black Holes. *J. Korean Phys. Soc.* **2008**, *52*, 986–991.
19. Escobedo, J. Greybody Factors. Master's Thesis, University of Amsterdam, Amsterdam, The Netherlands, 2008.
20. Parikh, M.K.; Wilczek, F. Hawking Radiation As Tunneling. *Phys. Rev. Lett.* **2000**, *85*, 5042–5045. <https://doi.org/10.1103/PhysRevLett.85.5042>.
21. Fleming, C.H. *Hawking Radiation as Tunneling; University of Maryland Department of Physics Technical Report*; UMD Physics: College Park, MD, USA, 2005.
22. Visser, M. Some general bounds for one-dimensional scattering. *Phys. Rev. A* **1999**, *59*, 427–438. <https://doi.org/10.1103/PhysRevA.59.427>.
23. Boonserm, P.; Visser, M. Bounding the greybody factors for Schwarzschild black holes. *Phys. Rev. D* **2008**, *78*, 101502. <https://doi.org/10.1103/PhysRevD.78.101502>.
24. Javed, W.; Hussain, I.; Övgün, A. Weak deflection angle of Kazakov-Solodukhin black hole in plasma medium using Gauss-Bonnet theorem and its greybody bonding. *Eur. Phys. J. Plus* **2022**, *137*.
25. Hoekstra, H.; Bartelmann, M.; Dahle, H.; Israel, H.; Limousin, M.; Meneghetti, M. Masses of galaxy clusters from gravitational lensing. *Space Sci. Rev.* **2013**, *177*, 75–118.
26. Brouwer, M.M.; Demchenko, V.; Harnois-Déraps, J.; Bilicki, M.; Heymans, C.; Hoekstra, H.; Kuijken, K.; Alpaslan, M.; Brough, S.; Cai, Y.C.; et al. Studying galaxy troughs and ridges using weak gravitational lensing with the Kilo-Degree Survey. *Mon. Not. Roy. Astron. Soc* **2018**, *481*, 5189.
27. Vanderveld, R.A.; Mortonson, M.J.; Hu, W.; Eifler, T. Testing dark energy paradigms with weak gravitational lensing. *Phys. Rev. D* **2012**, *85*, 103518. <https://doi.org/10.1103/PhysRevD.85.103518>.
28. Keeton, C.R.; Kochanek, C.S.; Falco, E.E. The Optical Properties of Gravitational Lens Galaxies as a Probe of Galaxy Structure and Evolution. *Astrophys. J.* **1998**, *509*, 561–578. <https://doi.org/10.1086/306502>.
29. Bhadra, A. Gravitational lensing by a charged black hole of string theory. *Phys. Rev. D* **2003**, *67*, 103009. <https://doi.org/10.1103/PhysRevD.67.103009>.
30. Whisker, R. Strong gravitational lensing by braneworld black holes. *Phys. Rev. D* **2005**, *71*, 064004. <https://doi.org/10.1103/PhysRevD.71.064004>.

31. Chen, S.; Jing, J. Strong field gravitational lensing in the deformed Hořava-Lifshitz black hole. *Phys. Rev. D* **2009**, *80*, 024036. <https://doi.org/10.1103/PhysRevD.80.024036>.
32. Nandi, K.K.; Zhang, Y.Z.; Zakharov, A.V. Gravitational lensing by wormholes. *Phys. Rev. D* **2006**, *74*, 024020. <https://doi.org/10.1103/PhysRevD.74.024020>.
33. Eiroa, E.F.; Romero, G.E.; Torres, D.F. Reissner-Nordström black hole lensing. *Phys. Rev. D* **2002**, *66*, 024010. <https://doi.org/10.1103/PhysRevD.66.024010>.
34. Kumaran, Y.; Övgün, A. Weak Deflection Angle of Extended Uncertainty Principle Black Holes. *Chin. Phys. C* **2020**, *44*, 025101. <https://doi.org/10.1088/1674-1137/44/2/025101>.
35. Kumaran, Y.; Övgün, A. Deflection Angle and Shadow of the Reissner-Nordström Black Hole with Higher-Order Magnetic Correction in Einstein-Nonlinear-Maxwell Fields. *Symmetry* **2022**, *14*, 2054.
36. Werner, M.C. Gravitational lensing in the Kerr-Randers optical geometry. *Gen. Relat. Gravi.* **2012**, *44*, 3047.
37. Ishihara, A.; Suzuki, Y.; Ono, T.; Kitamura, T.; Asada, H. Gravitational bending angle of light for finite distance and the Gauss-Bonnet theorem. *Phys. Rev. D* **2016**, *94*, 084015. <https://doi.org/10.1103/PhysRevD.94.084015>.
38. Ishihara, A.; Suzuki, Y.; Ono, T.; Asada, H. Finite-distance corrections to the gravitational bending angle of light in the strong deflection limit. *Phys. Rev. D* **2017**, *95*, 044017. <https://doi.org/10.1103/PhysRevD.95.044017>.
39. Ono, T.; Ishihara, A.; Asada, H. Gravitomagnetic bending angle of light with finite-distance corrections in stationary axisymmetric spacetimes. *Phys. Rev. D* **2017**, *96*, 104037. <https://doi.org/10.1103/PhysRevD.96.104037>.
40. Crisnejo, G.; Gallo, E. Weak lensing in a plasma medium and gravitational deflection of massive particles using the Gauss-Bonnet theorem. A unified treatment. *Phys. Rev. D* **2018**, *97*, 124016. <https://doi.org/10.1103/PhysRevD.97.124016>.
41. Li, Z.; Övgün, A. Finite-distance gravitational deflection of massive particles by a Kerr-like black hole in the bumblebee gravity model. *Phys. Rev. D* **2020**, *101*, 024040. <https://doi.org/10.1103/PhysRevD.101.024040>.
42. Li, Z.; Zhang, G.; Övgün, A. Circular orbit of a particle and weak gravitational lensing. *Phys. Rev. D* **2020**, *101*, 124058. <https://doi.org/10.1103/PhysRevD.101.124058>.
43. Oort, J.H. The force exerted by the stellar system in the direction perpendicular to the galactic plane and some related problems. *Astron. Inst. Netherlands* **1932**, *6*, 249.
44. Zwicky, F. On the Masses of Nebulae and of Clusters of Nebulae. *Astrophys. J.* **1937**, *86*, 217.
45. Feng, J.L. Dark Matter Candidates from Particle Physics and Methods of Detection. *Astrophys. J. Suppl. Ser.* **2010**, *48*, 495–545.
46. Jarosik, N.; Bennett, C.L.; Dunkley, J.; Gold, B.; Greason, M.R.; Halpern, M.; Hill, R.S.; Hinshaw, G.; Kogut, A.; Komatsu, E.; et al. Seven-year wilkinson microwave anisotropy probe (WMAP\*) observations: sky maps, systematic errors, and basic results. *Astrophys. J. Suppl. Ser.* **2011**, *192*, 14.
47. Övgün, A. Deflection Angle of Photons through Dark Matter by Black Holes and Wormholes Using Gauss–Bonnet Theorem. *Universe* **2019**, *5*, 115. <https://doi.org/10.3390/universe5050115>.
48. Pantig, R.C.; Övgün, A. Dark matter effect on the weak deflection angle by black holes at the center of Milky Way and M87 galaxies. *Eur. Phys. J. C* **2022**, *82*, 391. <https://doi.org/10.1140/epjc/s10052-022-10319-8>.
49. Pantig, R.C.; Rodulfo, E.T. Weak deflection angle of a dirty black hole. *Chin. J. Phys.* **2020**, *66*, 691–702. <https://doi.org/10.1016/j.cjph.2020.06.015>.
50. Pantig, R.C.; Övgün, A. Black hole in quantum wave dark matter. *Fortsch. Phys.* **2022**, *2022*, 2200164. <https://doi.org/10.1002/prop.202200164>.
51. Pantig, R.C.; Övgün, A. Dehnen halo effect on a black hole in an ultra-faint dwarf galaxy. *JCAP* **2022**, *08*, 056. <https://doi.org/10.1088/1475-7516/2022/08/056>.
52. Akiyama, K.; Alberdi, A.; Alef, W.; Asada, K.; Azuly, R. First M87 Event Horizon Telescope Results. I. The Shadow of the Supermassive Black Hole. *Astrophys. J. Lett.* **2019**, *875*, L1,17. <https://doi.org/10.3847/2041-8213/ab0ec7>.
53. Akiyama, K.; Alberdi, A.; Alef, W.; Algaba, J.C.; Anantua, R.; Asada, K.; Azulay, R.; Bach, U.; Baczko, A.K.; Ball, D.; et al. First Sagittarius A\* Event Horizon Telescope Results. I. The Shadow of the Supermassive Black Hole in the Center of the Milky Way. *Astrophys. J. Lett.* **2022**, *930*, L12. <https://doi.org/10.3847/2041-8213/ac6674>.
54. Bardeen, J.M.; Press, W.H.; Teukolsky, S.A. Rotating Black Holes: Locally Nonrotating Frames, Energy Extraction, and Scalar Synchrotron Radiation. *Astrophys. J.* **1972**, *178*, 347–370. <https://doi.org/10.1086/151796>.
55. Synge, J.L. The Escape of Photons from Gravitationally Intense Stars. *Mon. Not. Roy. Astron. Soc.* **1966**, *131*, 463–466. <https://doi.org/10.1093/mnras/131.3.463>.
56. Luminet, J.P. Image of a spherical black hole with thin accretion disk. *Astron. Astrophys.* **1979**, *75*, 228–235.
57. Narayan, R.; Johnson, M.D.; Gammie, C.F. The Shadow of a Spherically Accreting Black Hole. *Astrophys. J.* **2019**, *885*, L33. <https://doi.org/10.3847/2041-8213/ab518c>.
58. Guo, Y.; Miao, Y.G. Charged black-bounce spacetimes: Photon rings, shadows and observational appearances. *Nucl. Phys. B* **2022**, *983*, 115938. <https://doi.org/10.1016/j.nuclphysb.2022.115938>.
59. Pantig, R.C.; Yu, P.K.; Rodulfo, E.T.; Övgün, A. Shadow and weak deflection angle of extended uncertainty principle black hole surrounded with dark matter. *Ann. Phys.* **2022**, *436*, 168722. <https://doi.org/10.1016/j.aop.2021.168722>.
60. Konoplya, R.A.; Zhidenko, A. Solutions of the Einstein Equations for a Black Hole Surrounded by a Galactic Halo. *Astrophys. J.* **2022**, *933*, 166. <https://doi.org/10.3847/1538-4357/ac76bc>.

61. Konoplya, R.A. Shadow of a black hole surrounded by dark matter. *Phys. Lett. B* **2019**, *795*, 1–6. <https://doi.org/10.1016/j.physletb.2019.05.043>.
62. Xu, Z.; Hou, X.; Gong, X.; Wang, J. Black Hole Space-time In Dark Matter Halo. *JCAP* **2018**, *09*, 038.
63. Xu, Z.; Gong, X.; Zhang, S.N. Black hole immersed dark matter halo. *Phys. Rev. D* **2020**, *101*, 024029.
64. Pantig, R.C.; Rodulfo, E.T. Rotating dirty black hole and its shadow. *Chin. J. Phys.* **2020**, *68*, 236–257. <https://doi.org/10.1016/j.cjph.2020.08.001>.
65. Javed, W.; Irshad, H.; Pantig, R.C.; Övgün, A. Weak Deflection Angle by Kalb-Ramond Traversable Wormhole in Plasma and Dark Matter Mediums. *Universe* **2022**, *8*, 599. <https://doi.org/10.3390/universe8110599>.
66. Javed, W.; Riaz, S.; Pantig, R.C.; Övgün, A. Weak gravitational lensing in dark matter and plasma mediums for wormhole-like static aether solution. *Eur. Phys. J. C* **2022**, *82*, 1057. <https://doi.org/10.1140/epjc/s10052-022-11030-4>.
67. Jusufi, K.; Jamil, M.; Zhu, T. Shadows of Sgr A\* black hole surrounded by superfluid dark matter halo. *Eur. Phys. J. C* **2020**, *80*, 354. <https://doi.org/10.1140/epjc/s10052-020-7899-5>.
68. Nampalliwar, S.; Kumar, S.; Jusufi, K.; Wu, Q.; Jamil, M.; Salucci, P. Modeling the Sgr A\* Black Hole Immersed in a Dark Matter Spike. *Astrophys. J.* **2021**, *916*, 116. <https://doi.org/10.3847/1538-4357/ac05cc>.
69. Berry, Thomas, A.S.; Visser, M. General class of “quantum deformed” regular black holes. *Universe* **2021**, *7*, 165.
70. Huang, H.; Yang, J. Charged Ellis wormhole and black bounce. *Phys. Rev. D* **2019**, *100*, 124063.
71. Franzin, E.; Liberati, S.; Mazza, J.; Simpson, A.; Visser, M. Charged black-bounce spacetimes. *J. Cosmo. Astropart. Phys.* **2021**, *2021*, 036.
72. Morris, M.S.; Thorne, K.S. Wormholes in space-time and their use for interstellar travel: A tool for teaching general relativity. *Am. J. Phys.* **1988**, *56*, 395–412. <https://doi.org/10.1119/1.15620>.
73. Hayward, S.A. Formation and Evaporation of Nonsingular Black Holes. *Phys. Rev. Lett.* **2006**, *96*, 031103. <https://doi.org/10.1103/PhysRevLett.96.031103>.
74. Guo, Y.; Miao, Y.G. Bounce corrections to gravitational lensing, quasinormal spectral stability and gray-body factors of Reissner-Nordström black holes. *arXiv* **2022**, arXiv:2201.02971.
75. Lobo, F.S.N.; Rodrigues, M.E.; Silva, M.V.d.S.; Simpson, A.; Visser, M. Novel black-bounce spacetimes: Wormholes, regularity, energy conditions, and causal structure. *Phys. Rev. D* **2021**, *103*, 084052. <https://doi.org/10.1103/PhysRevD.103.084052>.
76. Simpson, A.; Martín-Moruno, P.; Visser, M. Vaidya spacetimes, black-bounces, and traversable wormholes. *Class. Quantum Gravity* **2019**, *36*, 145007. <https://doi.org/10.1088/1361-6382/ab28a5>.
77. Gibbons, G.W.; Werner, M.C. Applications of the Gauss–Bonnet theorem to gravitational lensing. *Class. Quantum Grav.* **2008**, *25*, 235009.
78. Latimer, D.C. Dispersive light propagation at cosmological distances: Matter effects. *Phys. Rev. D* **2013**, *88*, 063517. <https://doi.org/10.1103/PhysRevD.88.063517>.
79. Gibbons, G.W.; Hawking, S.W. Cosmological event horizons, thermodynamics, and particle creation. *Phys. Rev. D* **1977**, *15*, 2738–2751. <https://doi.org/10.1103/PhysRevD.15.2738>.
80. Boonserm, P.; Visser, M. Bounding the Bogoliubov coefficients. *Ann. Phys.* **2008**, *323*, 2779–2798. <https://doi.org/10.1016/j.aop.2008.02.002>.
81. P, B. Rigorous Bounds on Transmission, Reflection and Bogoliubov Coefficients. Ph.D. Thesis, Victoria University Wellington, Wellington, New Zealand, 2009.
82. Ngampitipan, T.; Boonserm, P. Bounding the greybody factors for non-rotating black holes. *J. Mod. Phys. D* **2013**, *22*, 1350058.
83. Perlick, V.; Tsupko, O.Y.; Bisnovatyi-Kogan, G.S. Influence of a plasma on the shadow of a spherically symmetric black hole. *Phys. Rev. D* **2015**, *92*, 104031. <https://doi.org/10.1103/PhysRevD.92.104031>.
84. Pantig, R.C.; Övgün, A. Testing dynamical torsion effects on the charged black hole’s shadow, deflection angle and greybody with M87\* and Sgr. A\* from EHT. *Ann. Phys.* **2023**, *448*, 169197. <https://doi.org/10.1016/j.aop.2022.169197>.

**Disclaimer/Publisher’s Note:** The statements, opinions and data contained in all publications are solely those of the individual author(s) and contributor(s) and not of MDPI and/or the editor(s). MDPI and/or the editor(s) disclaim responsibility for any injury to people or property resulting from any ideas, methods, instructions or products referred to in the content.